Electronic Supplementary Material (ESI) for Materials Horizons.
This journal is © The Royal Society of Chemistry 2023

Supporting Information

Superior High-Temperature Capacitive Performance of PAEK Copolymer Composites Enabled by Interfacial Engineered Charge Traps

Xinyi Li[a], Yunchuan Xie[a], Jie Xiong[a], Bofeng Zhu[b], Xiao Zhang[b], Xinhua Duan[a], Bo Dong[c]*, Zhicheng Zhang[a]**

a Xi'an Key Laboratory of Sustainable Energy Materials Chemistry, National Innovation Platform (Center) for Industry-Education Integration of Energy Storage Technology, School of Chemistry, Xi'an Jiaotong University, Xi'an, P. R. China 710049

b National Key Laboratory of Science and Technology on Vessel Integrated Power System, Naval University of Engineering, Wuhan, P. R. China 430033.

c Chambroad Chemical Industry Research Institute Co., Ltd. Binzhou, P. R. China 256500.

Preparation and structural characterization of the composite dielectrics

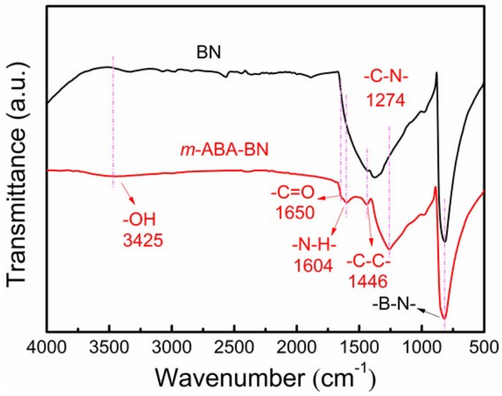

Figure S1. Fourier-transform infrared (FT-IR) spectra for BN and *m*-ABA-BN particles.

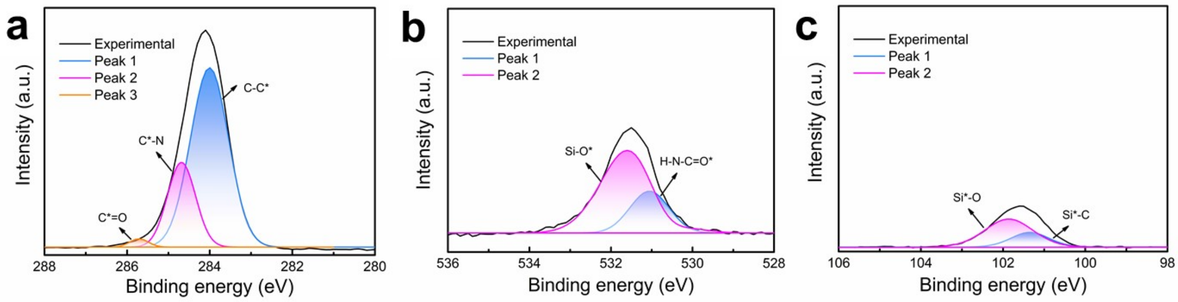

Figure S2. XPS plot of surface elements and chemical bonds of *m*-ABA-BN particles.

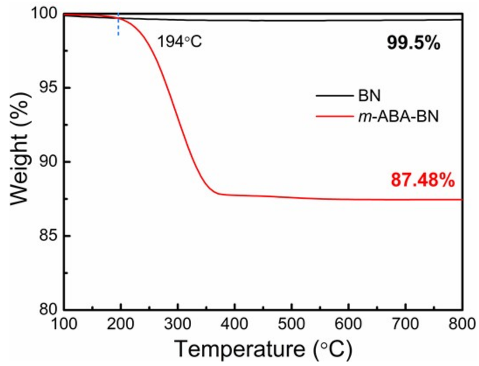

Figure S3. TGA curves of BN and *m*-ABA-BN particles.

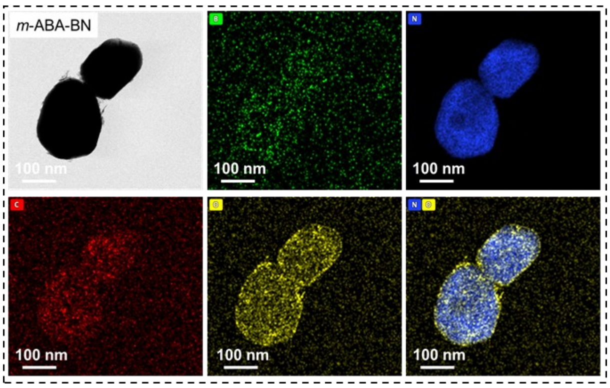

Figure S4. The elements distribution of *m*-ABA-BN.

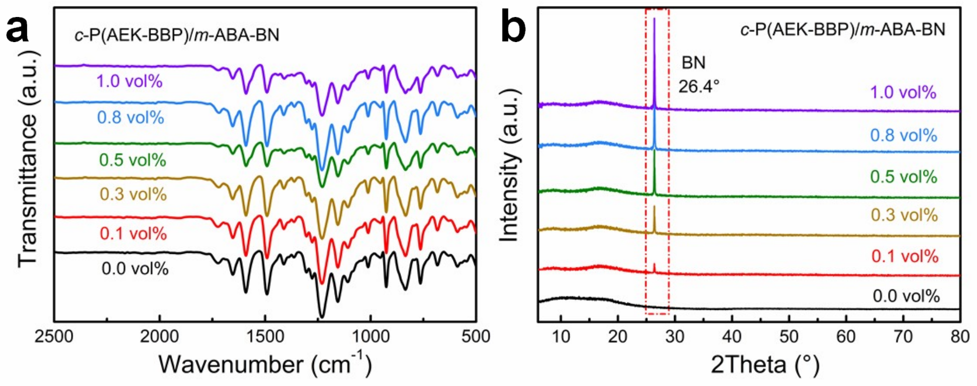

Figure S5. (a) FT-IR spectra and (b) XRD patterns of composite films with different *m*-ABA-BN contents.

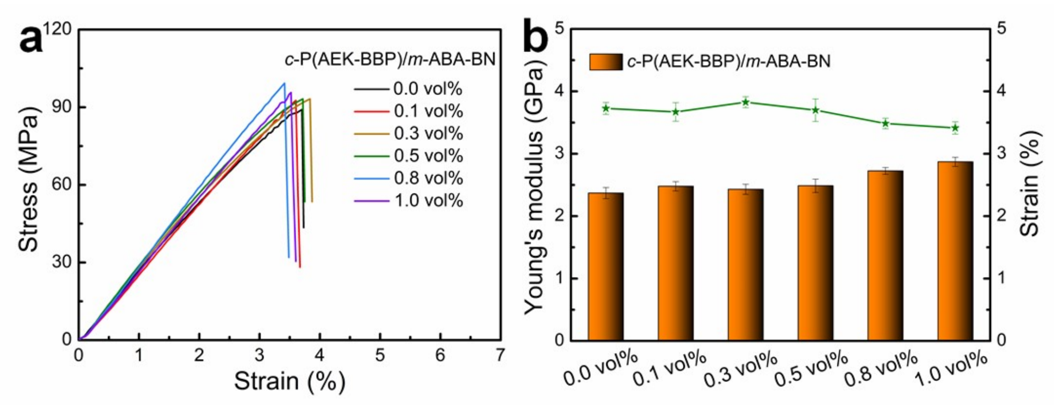

Figure S6. (a) Stress-strain curves and (b)Young's modulus of *c*-P(AEK-BBP)/*m*-ABA-BN with different *m*-ABA-BN contents.

Dielectric properties of the composites under varied electric fields

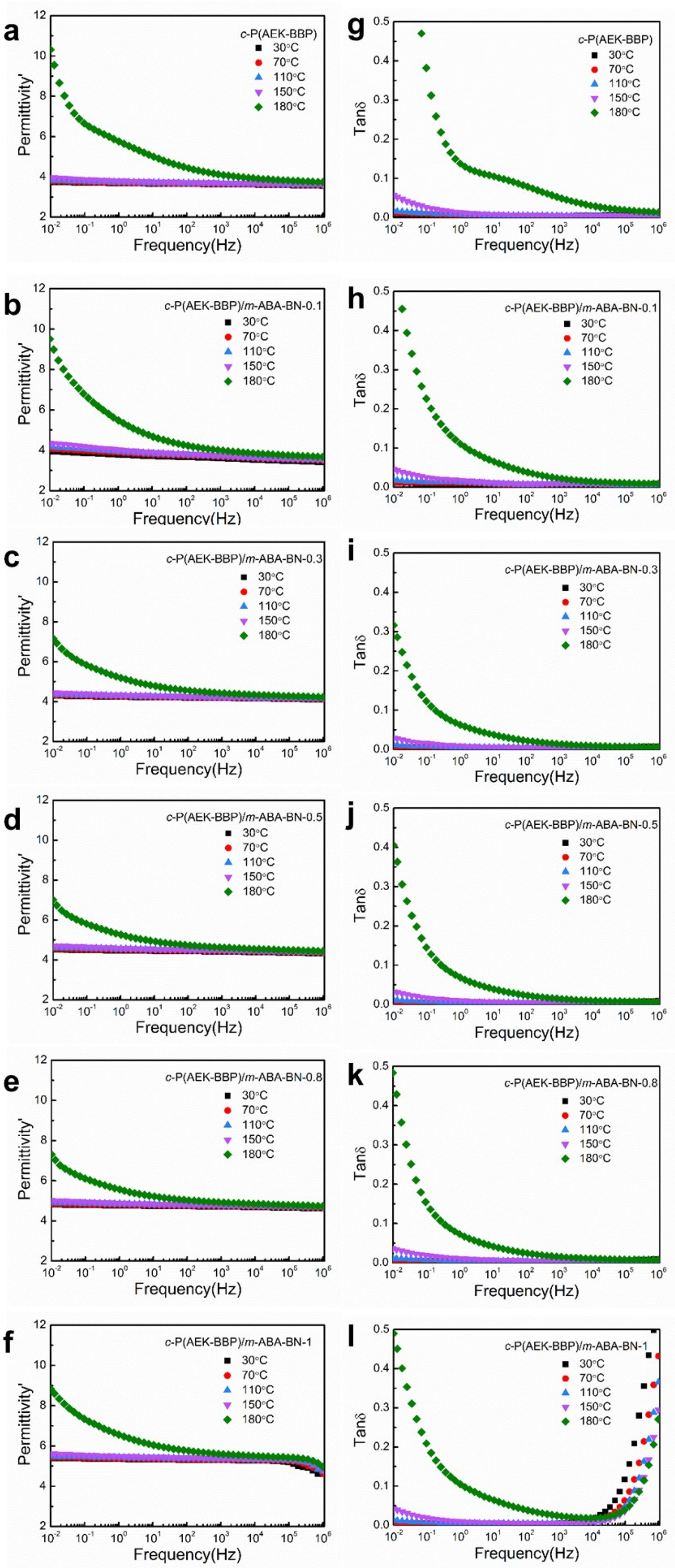

Figure S7. The permittivity (a)~(f) and loss factor (g)~(l) of the composite films with different *m*-ABA-BN contents as a function of frequencies at different temperatures.

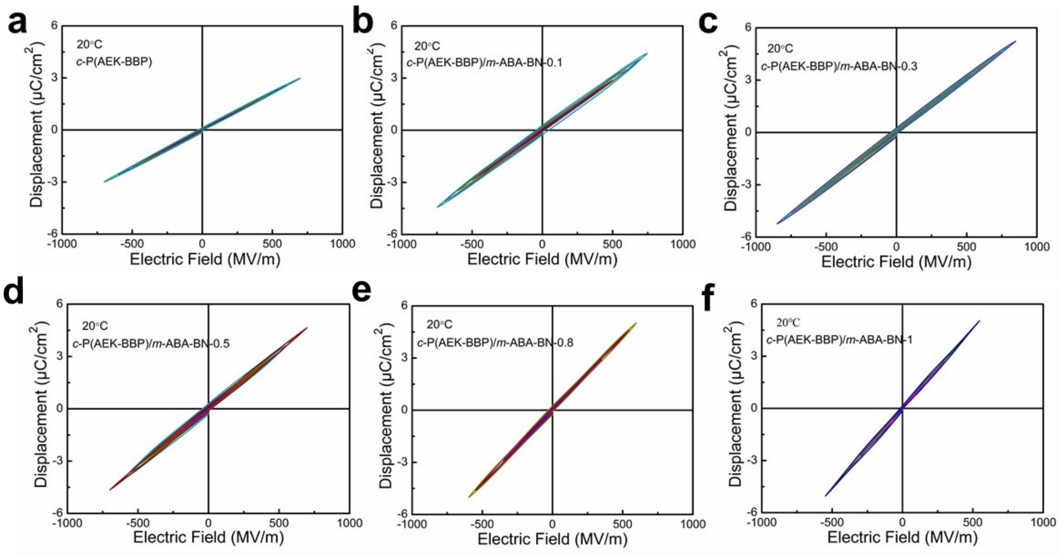

Figure S8. (a)~(f) *D*-*E* loops of *c*-P(AEK-BBP)/*m*-ABA-BN with different *m*-ABA-BN contents at room temperature.

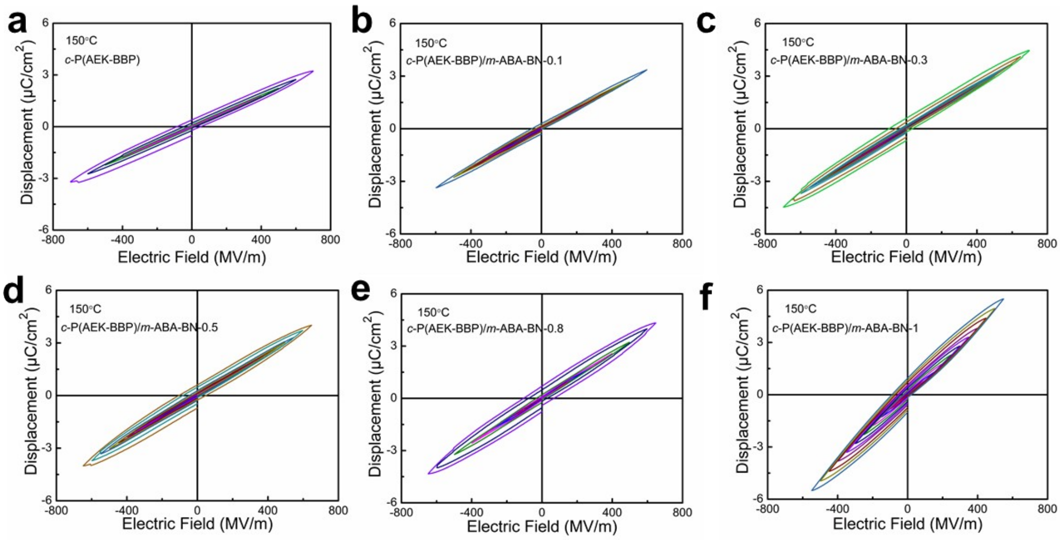

Figure S9. (a)~(f) *D*-*E* loops of *c*-P(AEK-BBP)/*m*-ABA-BN with different *m*-ABA-BN contents at 150 °C.

Capacitive performance of the composites under high electrical field at elevated temperature

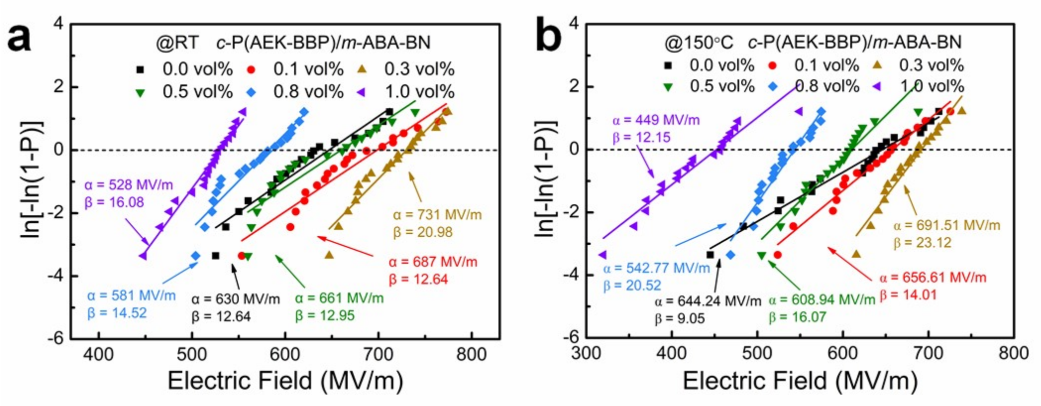

Figure S10. Weibull distribution plots of *c*-P(AEK-BBP) and composites with different *m*-ABA-BN contents (a) at room temperature and (b) 150 °C.

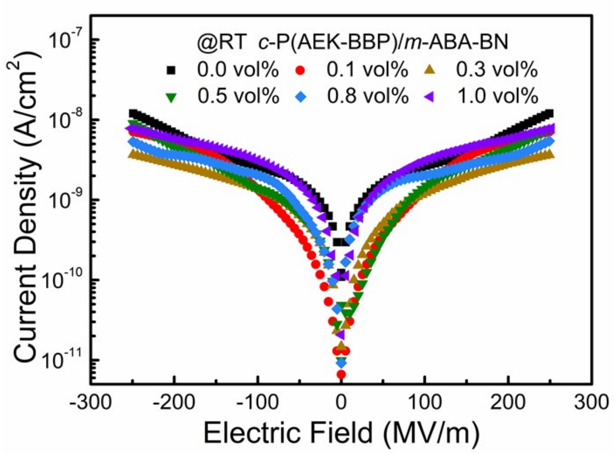

Figure S11. Leakage current density for *c*-P(AEK-BBP) and composites with different *m*-ABA-BN contents.

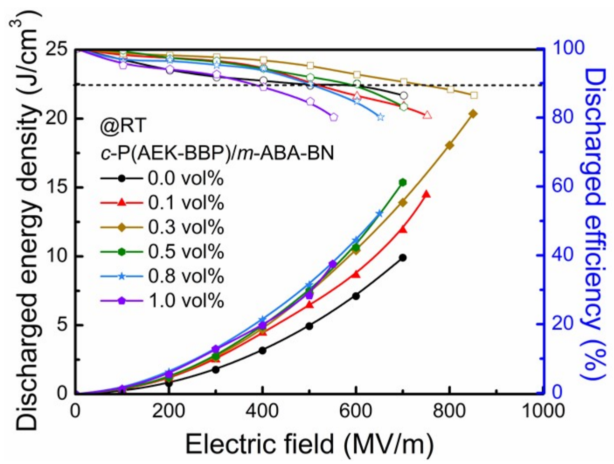

Figure S12. Discharged energy density and charge-discharge efficiency of *c*-P(AEK-BBP) and composites with varying *m*-ABA-BN contents as a function of the electric field.

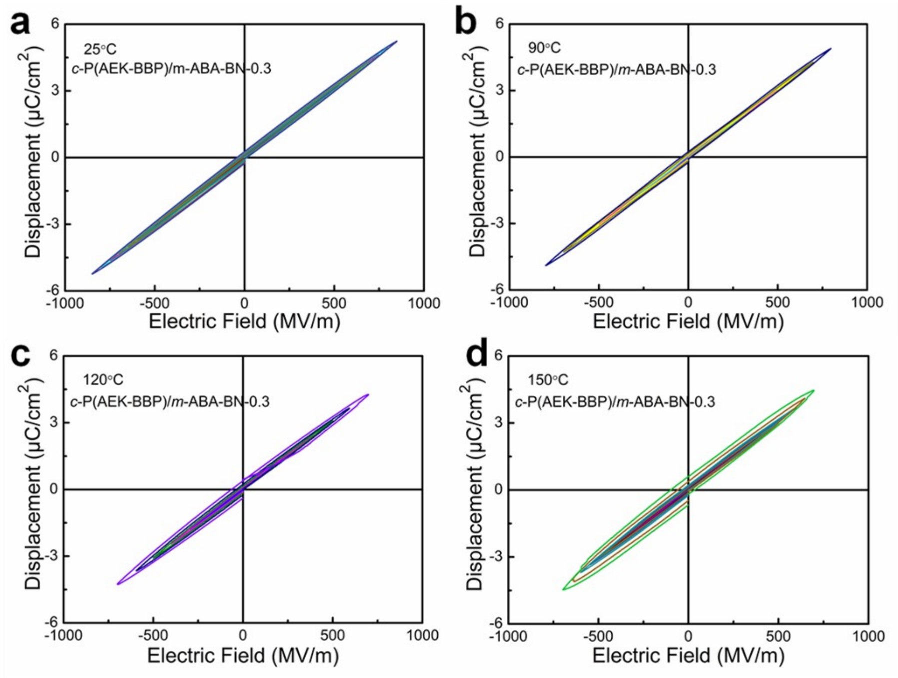

Figure S13. *D*-*E* loop of *c*-P(AEK-BBP)/*m*-ABA-BN-0.3 at (a) 25 ℃, (b) 90 ℃, (c) 120 ℃, (d) 150 ℃.

Charge transport mechanism of the composite dielectrics

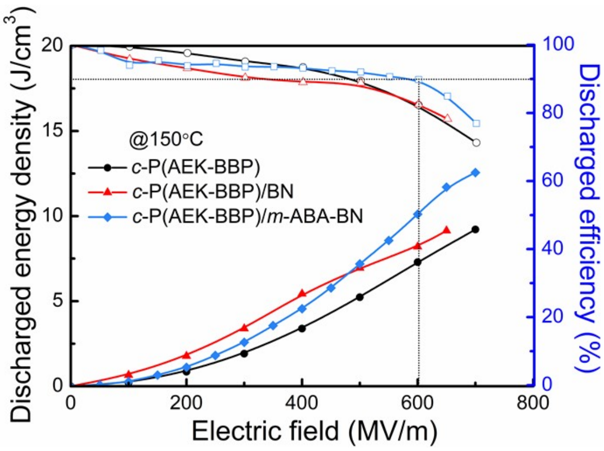

Figure S14. Discharged energy density and charge-discharge efficiency of *c*-P(AEK-BBP) and composites at 150 ℃ as a function of the electric field.

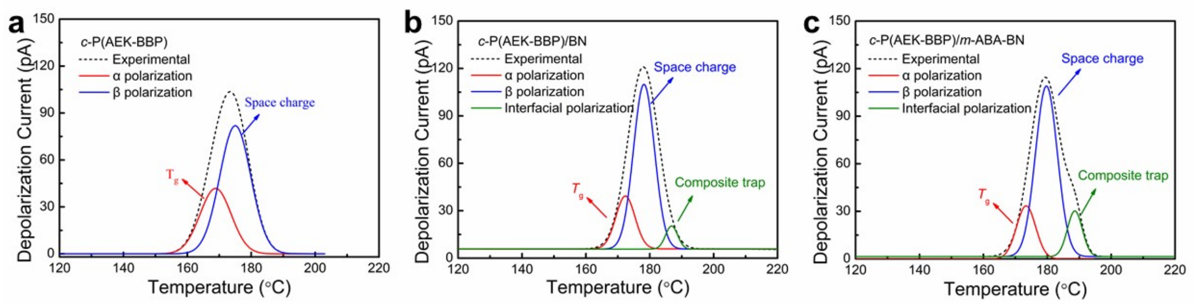

Figure S15. TSDC curves of (a) *c*-P(AEK-BBP), (b) *c*-P(AEK-BBP)/BN, and (c) *c*-P(AEK-BBP)/*m*-ABA-BN-0.3 film.